The Photodetachment Microscope

Christophe Blondel, Christian Delsart, and François Dulieu
Laboratoire Aimé-Cotton, Centre National de la Recherche Scientifique II, Bâtiment 505, F-91405 Orsay cedex, France
(Received 24 May 1996)

Br^- ions undergo photodetachment in the presence of an electric field. As a result of the photoexcitation process, the emitted electron's wave function extends to infinity, but inside a paraboloid elongated in the direction of the field. A position-sensitive detector set across the electron emission axis makes it possible to image the transverse factor of the atomic wave function. A ring pattern is observed, with a number of dark rings which is analogous to the first parabolic quantum number of the LoSurdo-Stark problem. [S0031-9007(96)01549-9]

PACS numbers: 32.80.Gc, 07.78.+s, 32.60.+i

Electrons that escape from an atom in the presence of an electric field undergo a uniform acceleration that makes their motion analogous to free fall. In the case of photodetachment from a negative ion, since attraction by the residual atom ceases at short distances from the core, the photoelectron really goes away as a free electron, and its trajectory will be a parabola. Varying the emission angle for a given value ϵ of the initial energy gives rise to a bunch of parabolae, the envelope of which, as represented in Fig. 1, is itself a paraboloid.

Photoionization of an atom or photodetachment of a negative ion are, of course, quantum processes, the description of which must be completed by a quantum-mechanical treatment. For this purpose, the parabolic cooordinates $\xi = r + z$ and $\eta = r - z$, defined from r the distance from the origin (i.e., the position of the nucleus), and z the coordinate along the direction of the applied field [1] are the most appropriate. Namely, for a free electron, as in the free-electron approximation of photodetachment, or for photoionization of the hydrogen atom, thanks to a particular symmetry of the Coulomb problem, the wave function of the outgoing electron can be factorized as a product of one-dimensional functions of every parabolic coordinate.

Parabolic coordinates also make the equation of the envelope paraboloid of the classical trajectories very simple. With $a = \epsilon/qF$ the maximum distance the electron of charge $-q$ can go up the external potential before being reflected by the field F, electron trajectories are confined inside the volume $\xi \leq 2a$. Moreover, if electrons are collected on a plane detector set at a distance d below the emission point, large enough so that $a \ll d$, they reach the detector at a parabolic coordinate $\eta = \xi + 2d$ which is practically constant, $\eta \simeq 2d$.

The semiclassical picture (Fig. 1) shows that every point of the plane inside the $\xi = 2a$ paraboloid can be reached by two distinct trajectories. An interference pattern is thus expected, the center of which corresponds to a maximum phase difference between the interfering paths. The maximum radius $R_{\max} = \sqrt{2a(2a + d)} \simeq 2\sqrt{ad}$ at which electrons can fall off axis corresponds to degenerate trajectories, hence to a zero phase difference.

In a rigorous quantum-mechanical description, the electron distribution on the detector is a picture of the atomic wave function dependence on coordinate ξ (and possibly the azimuthal coordinate φ) at $\eta = 2d$. The quantum distribution will actually extend beyond the $\xi = 2a$ limit, because of the exponentially decreasing presence probability of the particle in the region of negative ξ kinetic energy. Observing this wave function, which had never been achieved before, has been the aim of the present work.

From LoSurdo-Stark spectroscopy to the photodetachment microscope.—The electron current, hence the interference pattern, depends on the emission energy ϵ. As a consequence, the total photoionization cross section undergoes a modulation, as a function of the energy, that extends well beyond the zero-field ionization threshold. This modulation was first observed in the photoionization spectra of Rb [2], then with Na [3], Yb [4], and H [5]. Quantum calculations [6] quickly explained the paradox that such a structure appears in a spectral region where nothing can be observed but a flat continuum in the absence of external fields. But though the spatial density of photoelectron current was introduced together with the interference model of the structure [7], the idea came only a little later that this spatial distribution of electron density

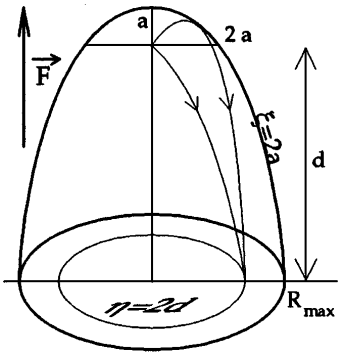

FIG. 1. Geometrical parameters of the photoionization or photodetachment problem in the presence of an electric field. For radii $R < R_{\max} \simeq 2\sqrt{ad}$ every point of the detector can be reached by two distinct trajectories.

could actually be observable, if one managed to build a "photoionization microscope" [8].

The dimension of the photoelectron pattern, however, makes the experiment with neutral atoms a difficult one. As a remarkable property of the LoSurdo-Stark problem, the interval i between adjacent bright rings is an invariant, but of the detection distance d: $i \approx \sqrt{da_0}$, with a_0 the Bohr radius. A spatial resolution of the order of 10 μm would thus be necessary to make the pattern visible in an experimental chamber of reasonable size (less than 1 m of uniform electric field), which explains why nobody ever observed it.

Negative ions, on the other hand, behave in a different way. Because they have no Rydberg series, only low values of the internal quantum numbers are associated with the detachment threshold. The energy of the photodetachment threshold is not much lowered by the electric field, so $\epsilon = 0$ corresponds only to the beginning of the oscillation of the photodetachment cross section [9]. Correspondingly, the number of rings between $R = 0$ and $R_{\max}$ can be much smaller than in the photoionization problem, and the ring interval i will be inversely greater, which makes the photodetachment case a more favorable one for the observation of the interference.

From the recent theoretical papers about photodetachment in an electric field [10–12], one can draw analytic formulas that directly estimate the maximum phase difference and distance between rings of the photodetachment pattern. We have used them in Fig. 2 to map out the observation conditions of the ring pattern in a photodetachment microscope, in the ϵ against F plane. Though the studied phenomenon occurs at any values of the electric field and excitation energy, practical conditions that the ring interval be larger than 100 μm and that the number of rings be larger than 1 make the useful domain surprisingly narrow. A natural limitation is imposed, in the direction of small energies, by the finite energy resolution of the excitation system.

Experimental setup.—A Br^- ion beam is formed from a hot cathode discharge source fed with potassium bromide, with argon as a buffer gas. A Wien velocity filter, steering, and collimating electrostatic optics bring 3 nA of pure Br^- into the interaction region, isotopically enriched either with $^{79}Br^-$ or with $^{81}Br^-$, with a maximum ratio of 80%.

The interaction chamber is drawn in Fig. 3. Since the position of the photodetached ion is the essential parameter that determines the final position of the photoelectron pattern, great care must be taken to make the transverse dimensions of the photodetachment zone as small as possible, in order not to blur the electron image. The excitation laser is thus set as parallel as possible to the electric field (without impinging on the electron detector) that is with a 3° angle, and focused onto the ion beam with a waist diameter of about 50 μm.

Threshold photodetachment of Br^- is obtained at wavelengths around 368.50 nm [13]. About 20 mW of CW single-mode radiation at this wavelength are produced by an intracavity frequency-doubled titanium-sapphire laser. The 93° incidence angle of the laser beam onto the 1 keV ion beam results in a positive Doppler shift of 0.23 cm^{-1}.

After a 51 cm flight, a photoelectron is detected by a stack of five microchannel plates followed by a resistive anode encoder [14]. With the help of a PC computer, photoelectron counts are made into histograms in a grid of 26 μm $\times$ 26 μm pixels, with a spatial resolution of 65 μm. A few hundred electrons are received per second, which is far below the maximum counting rate of the detector, but the conditions shown on Fig. 2 bind us to very low energies above the detachment threshold, which, because of the Wigner law [15], inevitably makes the detachment cross section also very low.

Results.—Figure 4 gives an example of a recorded electron image. The outer bright ring only results from the accumulation of photoelectrons at the maximum radius $R_{\max}$. This is a classical effect: while flying to

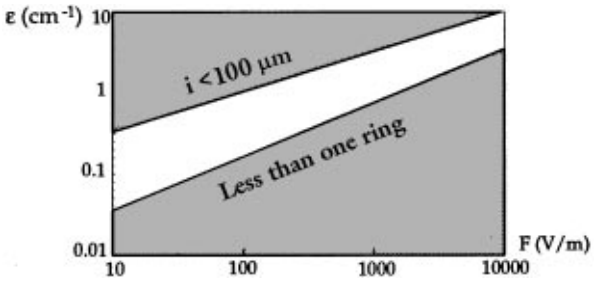

FIG. 2. Log-log diagram of the electron kinetic energy ϵ vs applied electric field F. The free area is where more than one ring will be observed, with a ring interval larger than 100 μm, assuming a detection distance $d = 0.5$ m.

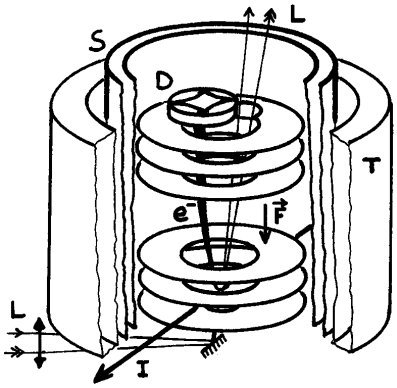

FIG. 3. Interaction chamber. The electric field, from the interaction zone to the detector (D) is produced by parallel stainless-steel plates, with a central hole of 27 mm in diameter. The laser beam (L) is sent onto the ion beam (I) with an angle of 93°. The chamber is shielded against the earth magnetic field by a double μ-metal layer (S), and surrounded by a liquid nitrogen tank (T) to reduce the residual pressure.

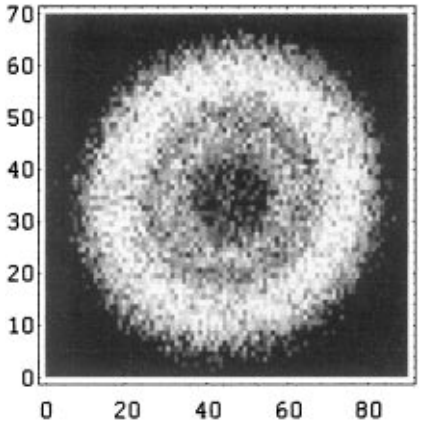

FIG. 4. Photodetachment pattern of $^{81}Br^-$ obtained within a 120 V/m electric field, with an excitation wave number of 27 129.39 cm^{-1}. The scales are pixel numbers. The mean diameter of the ring pattern is about 2 mm. Distortion is produced by the kinetic energy dispersion of the ion beam.

the detector, the photoelectron charge distribution expands spherically. Projection onto the detector would yield an infinite density at every point where the projection direction is parallel to the projected sphere, as is the case over the whole circle $R = R_{max}$. Finite spatial resolution and quantum penetration into the $\xi = 2a$ barrier transform this singularity into a finite maximum.

The inner bright ring, on the other hand, cannot be explained by classical projection arguments, nor by the hyperfine structure of neutral bromine. Figure 5 shows the radial histogram of the electron counts shown in Fig. 4, and the four different R_{max} corresponding to the four hyperfine detachment subthresholds of $^{81}Br^-$, with their respective contribution. The secondary rings that hyperfine structure would produce, if we had a resolution good enough to see them, would be outer rings, not an inner ring as here observed.

Data are on the contrary well reproduced by a quantum computation, assuming a 0.009 cm^{-1} energy resolution (due to residual Doppler broadening), a 120 μm overall spatial resolution, and an excitation energy $\epsilon = 0.43\ cm^{-1}$ consistent with the measured wavelength $\lambda = 368\,499$ pm if one takes the experimental uncertainty $\pm 0.04\ cm^{-1}$ into account. This uncertainty is essentially due to the unperfectly known incidence angle, and to the uncertainty on the energy of the detachment threshold itself [13]. The total phase of the oscillations, from R_{max} to zero, seems to be 1.2 times what theory predicts [11], which may be the signature of a nonhydrogenic ion as seen through the photodetachment microscope.

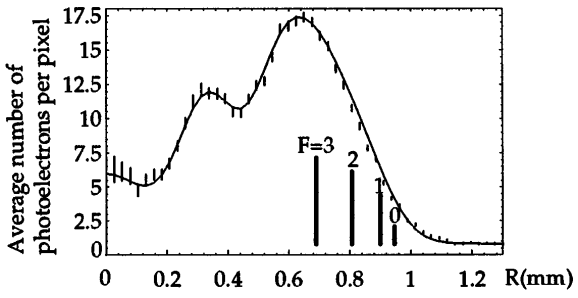

FIG. 5. Average radial histogram of the number of counted electrons, compared to its computed counterpart. The vertical bars show the radii R_{max} of the four possible hyperfine states of the residual atom, with heights proportional to their respective contributions. A purely classical calculation (projection of uniformly charged concentric spheres) would not produce any short-radius oscillation.

Because of the initial ion velocity, the photoelectron image is shifted with respect to the photodetachment origin by several millimeters in the ion beam direction. Dispersion of the ion beam kinetic energy thus produces some distortion of the electron image that we have compensated in Fig. 4 by using slightly different scales. Taking the 0.6 mm ion beam diameter into account, the 3° deviation of the laser beam from perfect parallelism with the field is also responsible for a 30 μm elongation along the ion beam direction.

Electron microscopes, either transmission [16] or scanning tunneling microscopes [17], now show individual atoms. At the ultimate level of electron holography [18], a "highly modified, computer processed, derivative of the original holographic intensity function" [19] even reveals the presence of several atomic shells, but no electron microscope ever showed the nodes and antinodes of the electron atomic wave functions.

Yet nodes and antinodes can be seen in photoelectron [20] or even tunnel electron [17] angular distributions, but these are purely angular wave functions that only deal with the balance between the allowed angular momentum eigenvalues of the electron state. Despite the interest such an information can have in the case of multiphoton excitation [21], this does not show anything about the radial motion of the electron.

Applying an electric field $\vec{F}$ to an atom here makes the situation different. The spherical symmetry of the atomic problem is broken, so that separation between radial and angular motion no longer takes place. This is taken as an advantage to bring radial information out to large distances from the core. Separability of the motion in parabolic coordinates guarantees that the large distance interferogram faithfully reproduces the ξ wave function as it was when the electron just exited the atom. Since the total dimension of this original wave function is a, with a of the order of half a micrometer in our experiment, the machine can well be named a "microscope."

Br^- ions have been chosen because their ground state is a $J = 0$ state, which makes the excitation start from a single quantum state. This may not be absolutely necessary. Despite its ground state degeneracy, $^{16}O^-$ would also detach into an s wave, with the advantage of having no hyperfine structure. Thanks to the much simpler image structure, effects of purely quantum nature could become

directly visible, such as the presence of electrons beyond R_{max}. Moreover, O^- detachment threshold is 1.461 11 eV [22], which makes photodetachment feasible with the fundamental Ti:Sa laser, i.e., 100 times more laser power. Since nearly no background is produced by the laser alone (nearly all of the electron background comes from collisional detachment of the ion beam onto the residual gas of the interaction chamber), an O^- photodetachment experiment can be expected to offer much shortened acquisition times, and a better signal-to-noise ratio.

Future studies should also investigate whether the uniform electric field region can be extended into a magnifying electric field configuration, which could be the way to making a photoionization microscope for neutral atoms. The sensitiveness of the recorded images to the freed electron energy makes it likely that this instrument could be used for high precision measurements of ionization potentials as well as of detachment energies.

Using an electron detector with a high spatial resolution to study photodetachment in an electric field, we have directly visualized the nodes and antinodes of a parabolic wave function. This is, to our knowledge, the first direct observation of an atomic wave function of at least partially radial nature, in contradistinction with the purely angular distributions usually recorded in photoionization or photodetachment studies. The coherence of the photoelectron bunch may also give rise to new interference studies.

We gratefully acknowledge discussions with V. D. Kondratovich and V. N. Ostrovskii. We also wish to thank M. Mellon, of Quantar Technology, for his continuous interest and support in the operation of the detector, and I. Yu. Kiyan for his criticism of the manuscript. This work has been supported by the D.R.E.T. office of our Ministère de la Défense under Contract No. 94-076.

[1] H. A. Bethe and E. E. Salpeter, *Quantum Mechanics of One- and Two-Electron Atoms* (Springer-Verlag, Berlin, Göttingen, Heidelberg, 1957); for recent developments on the LoSurdo-Stark problem see also D. A. Harmin, in *Atoms in Strong Fields,* edited by C. A. Nicolaides, C. W. Clark, and M. H. Nayfeh (Plenum Press, New York and London, 1990), p. 61; M. H. Nayfeh, D. Humm, and K. Ng, *ibid.,* p. 133; H. J. Silverstone, *ibid.,* p. 295.

[2] R. R. Freeman, N. P. Economou, and G. C. Bjorklund, Phys. Rev. Lett. **41**, 1463 (1978).

[3] T. S. Luk, L. DiMauro, T. Bergeman, and H. Metcalf, Phys. Rev. Lett. **47**, 83 (1981).

[4] C. Blondel, R.-J. Champeau, and C. Delsart, J. Phys. B **18**, 2403 (1985).

[5] W. L. Glab and M. H. Nayfeh, Phys. Rev. A **31**, 530 (1985); W. L. Glab, K. Ng, D. Yao, and M. H. Nayfeh, Phys. Rev. A **31**, 3677 (1985).

[6] E. Luc-Koenig and A. Bachelier, Phys. Rev. Lett. **43**, 921 (1979); J. Phys. B **13**, 1743 (1980); **13**, 1769 (1980).

[7] I. I. Fabrikant, Zh. Eksp. Teor. Fiz. **79**, 2070 (1980) [Sov. Phys. JETP **52**, 1045 (1980)].

[8] Yu. N. Demkov, V. D. Kondratovich, and V. N. Ostrovskii, Pis'ma Zh. Eksp. Teor. Fiz. **34**, 425 (1981) [JETP Lett. **34**, 403 (1981)].

[9] H. C. Bryant *et al.*, Phys. Rev. Lett. **58**, 2412 (1987); N. D. Gibson, B. J. Davies, and D. J. Larson, Phys. Rev. A **47**, 1946 (1993); **48**, 310 (1993).

[10] M. L. Du, Phys. Rev. A **40**, 4983 (1989).

[11] V. D. Kondratovich and V. N. Ostrovskii, J. Phys. B **23**, 3785 (1990).

[12] I. I. Fabrikant, J. Phys. B **23**, 1139 (1990); **27**, 4545 (1994).

[13] C. Blondel, P. Cacciani, C. Delsart, and R. Trainham, Phys. Rev. A **40**, 3698 (1989).

[14] Model 3391 of Quantar Technology Inc., 3004 Mission Street, Santa Cruz, CA 95060.

[15] E. P. Wigner, Phys. Rev. **73**, 1002 (1948).

[16] J. C. H. Spence, *Experimental High-Resolution Electron Microscopy* (Oxford University Press, New York, 1988).

[17] C. J. Chen, *Introduction to Scanning Tunneling Microscopy* (Oxford University Press, New York, 1993).

[18] L. S. Bartell and C. L. Ritz, Science **185**, 1163 (1974).

[19] L. S. Bartell, Optik (Stuttgart) **43**, 373 (1975); **43**, 403 (1975).

[20] A. F. Starace, in *Corpuscles and Radiation in Matter I, Encyclopedia of Physics,* edited by W. Mehlhorn (Springer-Verlag, Berlin, 1982), Vol. 31, p. 1; J. A. R. Samson, *ibid.,* p. 123.

[21] C. Blondel, M. Crance, C. Delsart, and A. Giraud, J. Phys. II (France) **2**, 839 (1992); F. Dulieu, C. Blondel, and C. Delsart, J. Phys. B **28**, 3845 (1995); **28**, 3861 (1995).

[22] D. M. Neumark, K. R. Lykke, T. Andersen, and W. C. Lineberger, Phys. Rev. A **32**, 1890 (1985), with correction by C. Blondel, Phys. Scr. **T58**, 31 (1995).